Sensors & Actuators: B. Chemical 361 (2022) 131688

Contents lists available at ScienceDirect

Sensors and Actuators: B. Chemical

journal homepage: www.elsevier.com/locate/snb

Integrating peroxidase-mimicking NH_2-MIL-101(Fe) with molecular imprinting for high-performance ratiometric fluorescence sensing of domoic acid

Linjie Wang [a,1], Lejuan Wen [a,1], Shujun Zheng [a], Feifei Tao [c], Jie Chao [d], Fei Wang [a,b,*], Caolong Li [a,b,*]

[a] Department of Chemistry, School of Science, China Pharmaceutical University, Nanjing 211198, Jiangsu, PR China
[b] Cell and Biomolecule Recognition Research Center, School of Science, China Pharmaceutical University, Nanjing 211198, PR China
[c] Department of Chemistry and Chemical Engineering, Shaoxing University, Shaoxing 312000, PR China
[d] Key Laboratory of Environmental Medicine Engineering, Ministry of Education, School of Public Health, Southeast University, Nanjing, PR China

ARTICLE INFO

Keywords:
Domoic acid
Ratiometric fluorescent sensor
Peroxidase-like activity
Inner filter effect
Molecular imprinting technology

ABSTRACT

Ingestion of shellfish and water containing excessive domoic acid (DA) threatens human health tremendously, and even causes death in severe cases. Herein, we have integrated the bifunctional NH_2-MIL-101(Fe) with molecular imprinting to design a ratiometric fluorescent sensor for quantitative analysis of DA. In this research, NH_2-MIL-101(Fe) itself can supply an intrinsic peak at 452 nm, and trigger oxidation of *o*-phenylenediamine (OPD) to 2,3-diaminophenazine (DAP) with peak at 556 nm owing to its excellent peroxidase-like activity. The two signal probes that influence each other owing to the inner filter effect (IFE) can form a highly sensitive composite fluorescent probe. Additionally, the introduction of molecular imprinting technology (MIT) instead of expensive antibodies can endow the ratiometric fluorescent sensor outstanding selectivity and specificity toward DA. Thus, the proposed ratiometric fluorescent sensor exhibits outstanding sensitivity, super anti-interference ability, and excellent selectivity. The experimental results demonstrate that the sensor exhibits good performance for DA sensing in the scope of 0.01–10 μM with low limit of detection (LOD) as 8.2 nM. More attractively, the successful spike and recovery experiments in real samples with the complicated matrix indicate the considerable practical application promise of our proposed ratiometric fluorescent sensor.

1. Introduction

Domoic acid (DA) produced by certain Pseudo-nitzschia and Nitzschia marine diatoms is the main component of amnestic shellfish poison [1,2]. Dangerously, the DA can be enriched in seafoods and subsequently transferred to humans through the food chain, which can cause toxic symptoms such as vomiting, diarrhea, short-term memory loss, and even death [3,4]. In 1987, the death of human poisoning event caused by DA occurred on the east coast of Prince Edward Island, Canada [5]. Since then, poisoning incidents of human and higher animals caused by DA have been reported successively around the world. Given this, the strict standard for the maximum levels of DA has been set by many countries in shellfish meat (20 $\mu g \cdot g^{-1}$) [6]. Therefore, developing reliable and sensitive analytical strategies for the quantitative analysis of DA is of great significance for controlling the pollution of DA in water ecological environment and protecting human health.

In the past decades, quantitative detection of DA mainly depended on mouse bioassay [7], high performance liquid chromatography (HPLC) [8,9], high performance capillary electrophoresis (HPCE) [10,11], and enzyme-linked immunosorbent assay (ELISA) [12,13]. Recently, electrochemical detection [14,15], fluorescent sensors [16] and other rapid detection methods have also been reported. Among these means, fluorescent sensors have aroused special interest because of their easy operation, outstanding analysis capability, and visual readout [17,18]. Especially, the fluorescent sensors with ratiometric modes are ideal for low level marine toxins detection [19].

Nanozymes as the substitutes to biological enzymes have attracted considerable interest [20,21]. Recently, nanozymes have been

* Corresponding authors at: Department of Chemistry, School of Science, China Pharmaceutical University, Nanjing 211198, Jiangsu, PR China.
E-mail addresses: feiwang@cpu.edu.cn (F. Wang), licl@cpu.edu.cn (C. Li).
[1] Authors who equally contribute to this work

https://doi.org/10.1016/j.snb.2022.131688
Received 1 January 2022; Received in revised form 26 February 2022; Accepted 8 March 2022
Available online 11 March 2022

employed extensively for analyzing versatile targets from ions to small molecules, and living organisms due to their easy availability, low cost, and excellent stability [22,23]. Surprisingly, the analysis strategies based on nanozymes can generate amplified signals via catalytic reaction, conducive to achieving excellent analytical performance [24]. Currently, extensive nanomaterials are reported possessing enzyme-like activity, among which metal organic frameworks (MOFs) have attracted much interest because of their flexible design in the matter of composition and structure [25,26]. Interestingly, the combination of metal nodes and organic ligands can endow MOFs multiple functions. For instance, part of ligands utilized in preparation of MOFs supply appealing luminescence characteristics, which allow them to be employed as optical labels for sensing target analytes [27]. Besides, numerous MOFs with active metal redox couples have been reported to reveal enzyme-mimicking activities to catalyze substrate reaction, which can enhance analytical sensitivity via signal amplification of the catalytic reaction [28]. More interestingly, these attractive functions can be reasonably integrated into a framework to form a composite signal probe for target sensing, which is greatly expanding the application potential of MOFs [29]. Molecular imprinting is a vital biomimetic recognition technology to mimic the specific recognition function of antibodies and enzymes. Compared to biological antibodies and enzymes, molecularly imprinted materials reveal comparable selectivity and specificity for target analytes. More attractively, they additionally exhibit superiorities of good stability, simple preparation, and low price [30,31]. Consequently, the multifunctional MOF (composite signal probe) and molecular imprinting (identify component) are combined to fabricate an integrated sensor, which has great application prospects in the field of biochemical analysis.

In this work, we have integrated the bifunctional Fe-based MOF with molecular imprinting to design a fluorescent sensor with ratiometric mode for DA sensing. As presented in Scheme 1(A), the NH_2-MIL-101 (Fe) is synthesized via a simple solvothermal method by utilizing $FeCl_3.6\ H_2O$ as a metal node and 2-NH_2-1,4-BDC as a ligand. On the one hand, the employed 2-NH_2-1,4-BDC endows MOF with a peak at 452 nm, and on the other hand, the mixed valence metal node of Fe^{3+}/Fe^{2+} in the

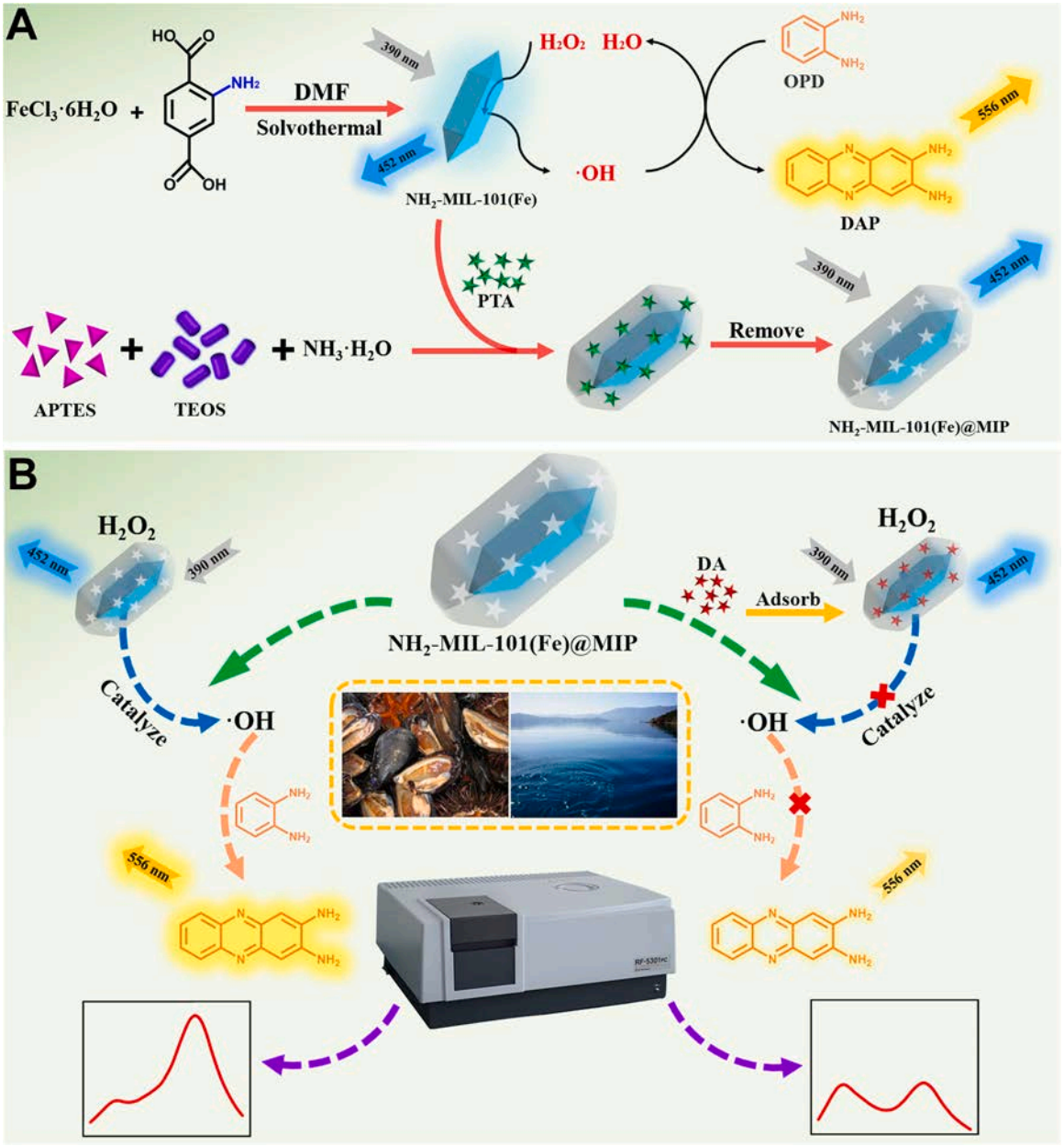

Scheme 1. The fabrication process of ratiometric fluorescent sensor (A) and sensing mechanism of DA (B).

MOF supplied excellent peroxidase-like activity to trigger oxidation of *o*-phenylenediamine (OPD) to the product 2,3-diaminophenazine (DAP) in the presence of H_2O_2. Fascinatingly, the DAP presents a distinct signal at 556 nm, which in turn represses the intrinsic peak (452 nm) owing to inner filter effect (IFE) [32]. Additionally, the NH_2-MIL-101(Fe)-based molecularly imprinted polymer (NH_2-MIL-101(Fe)@MIP) was prepared via a sol-gel strategy under the mild conditions (Scheme 1(A)). What should be mentioned is that the 1,3,5-pentanetrcarboxylicacid (PTA) is selected as an appropriate dummy template to replace the target molecule considering the high toxicity and expensive price of DA [33]. As demonstrated by Scheme 1(B), NH_2-MIL-101(Fe)@MIP displays similar optical properties and peroxidase-like activity to NH_2-MIL-101(Fe). After incubated with DA, the DA can specifically bind to the recognized cavities on NH_2-MIL-101(Fe)@MIP because of high selectivity and specificity offered by molecular imprinting technique (MIT), which blocks the passage of H_2O_2 through imprinted layer, and subsequently inhibits the production of hydroxyl radicals. Therefore, the fluorescence signal (556 nm) of DAP is suppressed, and the one (452 nm) is restored. Based on this strategy, an attractive ratiometric fluorescent sensor was fabricated and successfully used for rapid quantitative analysis of DA in lake water and shellfish samples.

2. Experimental

2.1. Chemicals and instrumentation

2-aminoterephthalic acid (2-NH_2-1,4-BDC), $FeCl_3.6\ H_2O$, N,N-dimethylformamide (DMF), acetic acid (HAc), acetone, ethanol, methanol, 3-aminopropyl-triethoxysilane (APTES), 1,3,5-pentanetrcarboxylicacid (PTA), ammonia (25%), tetraethoxysilane (TEOS), glutamic acid (Glu), glutaric acid (Glr), and glutamine (Gln) were purchased from Sinopharm Chemical Reagent. Domoic acid (DA) was acquired from National Research Council Canada. Na^+, Zn^{2+}, and other ionic standard solutions were all obtained from Guobiao (Beijing) Testing & Certification Co., Ltd. Unless otherwise stated, all purchased reagents were directly employed without purification. Ultrapure water was utilized throughout this research.

The fluorescence signals were recorded by Shimadzu RF-5301PC fluorescence spectrophotometer (Japan). The UV–vis spectra were obtained by Purkinje T6 spectrophotometer (China). Shellfish meat homogenate was prepared by a Wiggens D130 homogenizer (Germany). Scanning electron microscopy (SEM) images were captured by a Quanta 250 PEG microscope (Thermo Scientific). Fourier transform infrared (FT-IR) spectra were gained by Varian 3100 FT-IR (USA) spectrometer. X-ray photoelectron spectroscopy (XPS) spectra were acquired by a K-Alpha spectrometer (Thermo Scientific). The surface area and pore structure of prepared material were determined using a Quantachrome Autosorb IQ3 analyzer (USA).

2.2. Synthesis of NH_2-MIL-101(Fe)

The NH_2-MIL-101(Fe) was prepared by a simple solvothermal method [29]. Simply, $FeCl_3.6\ H_2O$ (2.5 mmol) as a metal node dissolved in 15 mL DMF was first transferred into 10 mL DMF containing 2-NH_2-1, 4-BDC (2.5 mmol) as an organic ligand. Then, 2.5 mL acetic acid was added into the above mixed solution to adjust the morphology of the prepared material. Subsequently, the mixture was transferred into a 50 mL autoclave and reacted at 120 ℃ for 12 h in the oven. After cooling to room temperature, the generated product was obtained by centrifugation and thoroughly washed by utilizing DMF and acetone for several times to remove residual metal ion and ligand. Finally, the obtained solid was dried at 50 °C.

2.3. Synthesis of NH_2-MIL-101(Fe)@MIP

The NH_2-MIL-101(Fe)@MIP was synthesized via a sol-gel strategy by utilizing TEOS as cross-linker, APTES as functional monomer, NH_2-MIL-101(Fe) as binding site, and PTA as dummy template. In detail, 50 mg MOF powder was first ultrasonically dispersed in 20 mL ethanol-water solution (1:1, V/V) and stirred for 10 min. Subsequently, 0.2 mL APTES, 20.4 mg (0.1 mmol) PTA, and 0.2 mL ammonia (25%) were added into above mixture successively and stirred for another 20 min. After that, 0.2 mL TEOS was added dropwise and stirred overnight in the dark. Afterwards, the synthesized solid was collected by centrifugation and eluted for several times with methanol/acetic acid (9:1, V/V) by centrifugal-ultrasonic circulation mode until PTA could be not discovered by the UV–vis spectrophotometer. Then the collected solid was washed with ultrapure water and ethanol to remove residual methanol and acetic acid, respectively. In the end, the product was dried in the dark. Besides, the NH_2-MIL-101(Fe)@NIP was prepared via a completely consistent procedure except that no dummy template molecule (PTA) was introduced.

2.4. The peroxidase-like activities of NH_2-MIL-101(Fe)

The peroxidase-like activities of the prepared materials were photometrically explored by utilizing OPD or TMB as substrate. All UV–vis spectra were performed by Purkinje T6 spectrophotometer (China). Specifically, 2.77 mL NaAc-HAc buffer (0.2 M, pH 4.0), 0.03 mL NH_2-MIL-101(Fe) aqueous dispersion (1 mg mL^{-1}), 0.1 mL H_2O_2 (0.98 M), and 0.1 mL TMB (5 mM) or OPD (10 mM) were added into a 5 mL plastic centrifuge tube in order, and reacted for 20 min. Finally, the above mixture was measured by UV-Vis. Additionally, the same experiment process was adopted to explore the peroxidase-like activity of NH_2-MIL-101(Fe)@MIP and NIP.

2.5. Ratiometric fluorescent sensing of DA

The ratiometric fluorescent sensing of DA was conducted by Shimadzu RF-5301PC fluorescence spectrophotometer. In detail, 0.1 mL NH_2-MIL-101(Fe)@MIP aqueous dispersion (1 mg mL^{-1}) and 0.1 mL various levels of DA were mixed in a 5 mL plastic centrifuge tube, and then incubated for 10 min. Subsequently, 2.6 mL NaAc-HAc buffer, 0.1 mL H_2O_2 (0.98 M), and 0.1 mL OPD (10 mM) were added to the above solution, and reacted for 20 min. Afterwards, the above mixed solution was measured by fluorescence spectrophotometer. The excitation and emission wavelength slit widths were set at 10 nm, and the sensitivity was set to high. The excitation wavelength was set to 390 nm, and the fluorescence intensities at 452 nm and 556 nm were determined. Finally, the relationship between F_{556}/F_{452} and the level of DA was investigated. The above tests were all carried out three times.

2.6. Analysis of DA in actual samples by the fabricated ratiometric fluorescent sensor

To evaluate the practical application potential of the fabricated ratiometric fluorescent sensor, the sensor was adopted to analyze DA in lake water and shellfish samples by spike and recovery test. The shellfish were acquired from the local seafood market, and the lake water was obtained from “Jing hu”, a lake on the campus of China Pharmaceutical University. These lake water and shellfish were analyzed by the fabricated ratiometric fluorescent sensor after a series of pretreatments. The details are depicted in Supporting Information (SI).

3. Results and discussion

3.1. Preparation and characterization of NH_2-MIL-101(Fe)

The NH_2-MIL-101(Fe) was prepared via a simple solvothermal method by utilizing $FeCl_3.6H_2O$ as a metal node and 2-NH_2-1,4-BDC as a ligand (Fig. 1A), and the material was characterized by several techniques. As displayed in XRD patterns (Fig. 1B), the several strong feature

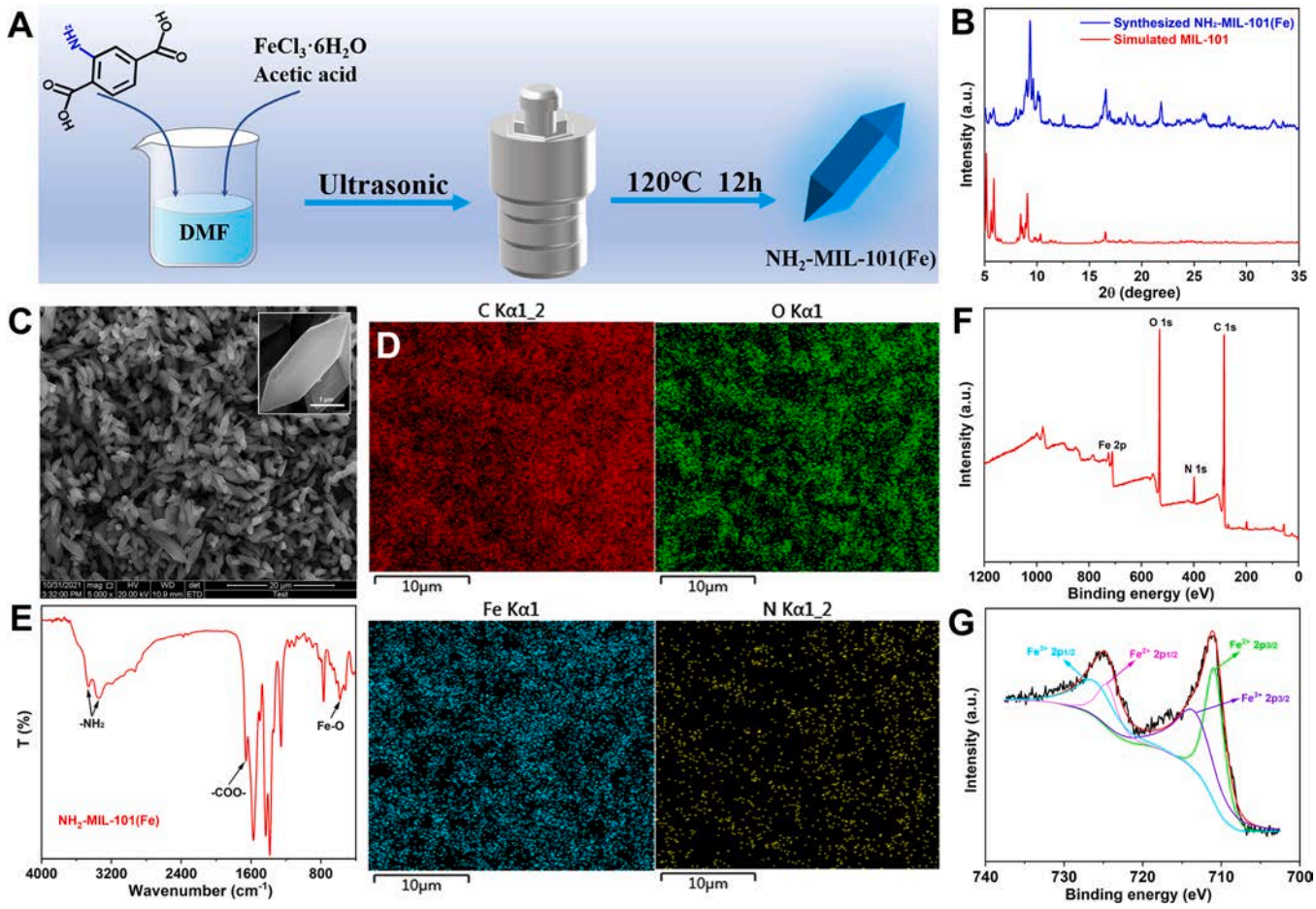

Fig. 1. (A) The synthesis route of NH_2-MIL-101(Fe). (B) The XRD spectra of prepared material and simulated MIL-101. (C) The SEM images and (D) the corresponding elemental mappings of C, O, Fe, and N elements. (E) The FT-IR spectrum. (F) The full XPS and (G) Fe 2p XPS.

peaks of synthesized product are generally in agreement with those of simulated MIL-101, and the XRD pattern of prepared material is almost consistent with those of NH_2-MIL-101(Fe) in some reported literatures [29,34]. The Fig. 1C and Fig. S1 display that the synthesized material presents the uniform almond-like shape, and the corresponding elements of C, O, Fe, and N are distributed evenly throughout the obtain product (Fig. 1D). The surface groups of prepared material were analyzed by FT-IR. As depicted in Fig. 1E, the FT-IR peaks at 3340 and 3460 cm^{-1} should be ascribed to the N-H stretching vibration, and the distinct peak at around 1650 cm^{-1} is assigned to carboxyl in the MOF. Besides, a peak signal at about 570 cm^{-1} should be ascribed to Fe–O bond vibration [35]. The full XPS result (Fig. 1F) also suggests the presence of Fe, O, C, and N in the synthesized material, and the Fe 2p XPS curve (Fig. 1G) can be divided into four peaks. The peaks at 714.0 eV and 726.6 eV should be ascribed to Fe(III), and the peaks at 711.0 eV and 724.7 eV should be attributed to Fe(II) [36]. Accordingly, the mixed valence states of Fe(II)/Fe(III) coexist on the surface of NH_2-MIL-101(Fe), which will endow the MOF with good peroxidase-like activity. All above results well confirm the successful synthesis of this material.

3.2. NH_2-MIL-101(Fe)@MIP preparation and characterization

Subsequently, the NH_2-MIL-101(Fe)@MIP was synthesized via a sol-gel strategy under the mild conditions (Fig. 2A), and the obtained product was characterized by several characterization instruments. Firstly, different ratios of functional monomer (APTES) and crosslinking agent (TESO) were tested to optimize the fluorescence properties of the NH_2-MIL-101(Fe)@MIP. The fluorescence intensities at 556 nm of NH_2-MIL-101(Fe)@MIP + DA + H_2O_2 + OPD and NH_2-MIL-101(Fe)@MIP + H_2O_2 + OPD systems were measured and compared. As depicted in Table S1, the optimal performance sensor uses NH_2-MIL-101(Fe)@MIP made from 200 μL APTES and 200 μL TEOS. The optimized NH_2-MIL-101(Fe)@MIP preparation scheme was employed in the following experiments. As displayed in Fig. S2, the several main feature peaks of NH_2-MIL-101(Fe) are observed in prepared imprinted polymers. However, the intensity of the feature peaks decreases significantly after imprinting, which is due to the coating of the imprinting layer. These results verify the successful imprinting process. The micromorphology of synthesized material is illustrated by SEM, and the corresponding images demonstrate the oval-like structure of NH_2-MIL-101(Fe)@MIP. Simultaneously, the rough molecularly imprinted layer can be observed distinctly (Fig. 2B). Additionally, the elemental mappings of NH_2-MIL-101(Fe)@MIP were studied. As depicted in Fig. 2 C, the related elements are distributed evenly throughout the prepared product. Besides, the NH_2-MIL-101(Fe)@NIP reveals similar micromorphology and element distribution to NH_2-MIL-101(Fe)@MIP. However, the overall micromorphology of NH_2-MIL-101(Fe)@MIP is relatively uniform (Fig. S3). These evidences strongly indicate that the imprinted layer is successfully formed. The FT-IR was utilized to study the surface groups of prepared imprinted polymers. As presented in Fig. 2D, the clear peak signals at 460 and 785 cm^{-1} originate from the Si–O vibrations and the distinct peak at 1055 cm^{-1} is ascribed to asymmetric Si–O–Si stretching, certifying the existence of SiO_2 imprinted layer. Meanwhile, the characteristic peaks at 1560 and 3440 cm^{-1} are N-H stretching vibration and the peak at approximately 2940 cm^{-1} should be assigned to C-H stretching

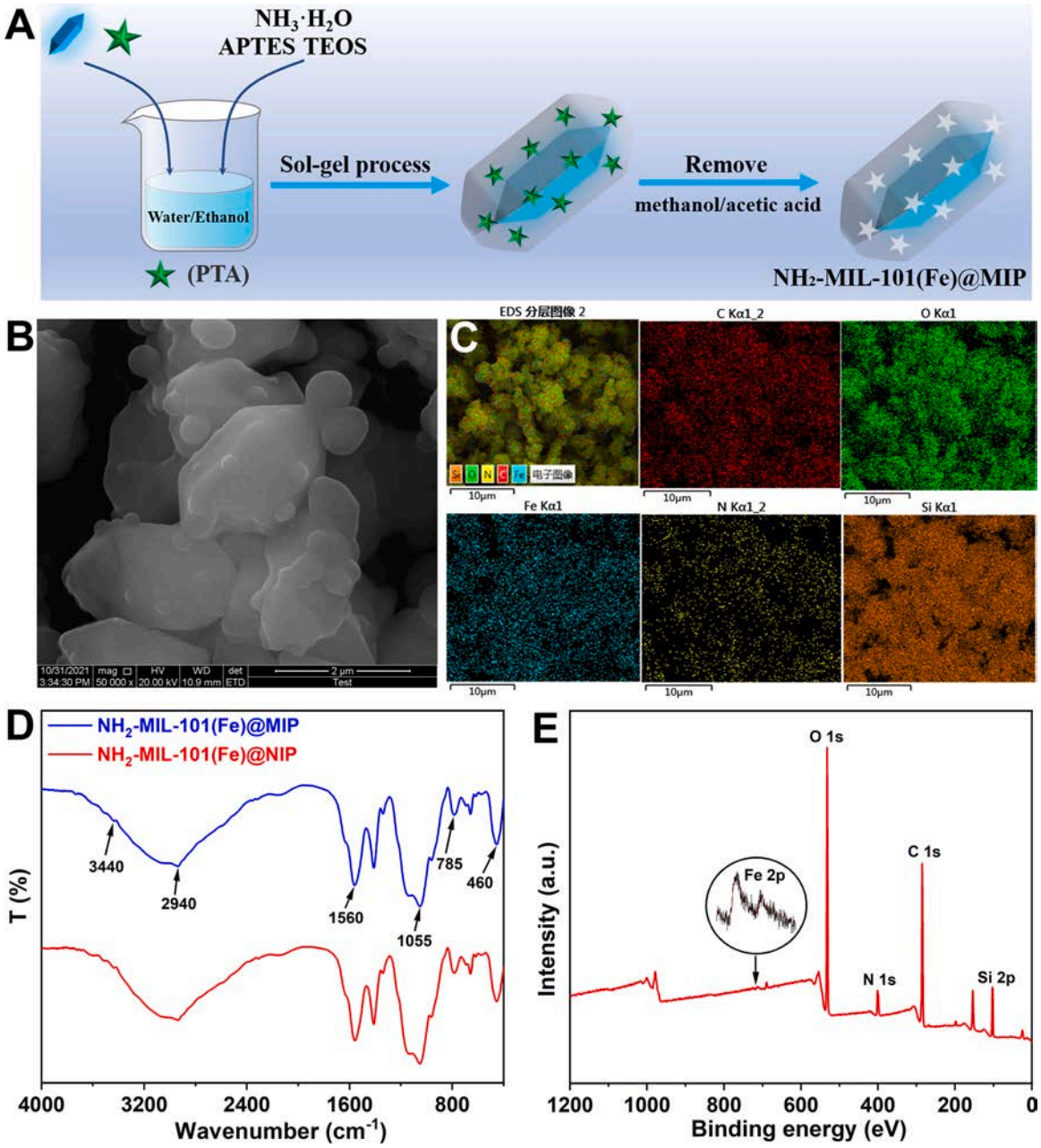

Fig. 2. (A) The synthesis route of NH_2-MIL-101(Fe)@MIP. (B) The SEM image of NH_2-MIL-101(Fe)@MIP, and (C) the corresponding elemental mappings of C, O, Fe, N, and Si elements. (D) The FT-IR spectra of NH_2-MIL-101(Fe)@MIP and NH_2-MIL-101(Fe)@NIP. (E) The full XPS of NH_2-MIL-101(Fe)@MIP.

vibration, indicating the existence of functional monomer (APTES) in the prepared imprinted polymers [37,38]. The full XPS spectrum (Fig. 1E) also demonstrates the existence of Fe, O, C, N, and Si elements, further illustrating that the imprinted layer is successfully coated on NH_2-MIL-101(Fe). However, the peak signal of Fe is extremely weak because extensive MOF are wrapped by imprinted layer, causing the measurement difficulty by XPS [39]. The surface area and pore structure of NH_2-MIL-101(Fe)@NIP and NH_2-MIL-101(Fe)@MIP were investigated by BET method. As displayed in Table S2, the specific surface area, average pore diameter, and pore volume of NH_2-MIL-101(Fe)@NIP are significantly smaller than those of NH_2-MIL-101(Fe)@MIP. These results further demonstrate many molecularly imprinted cavities on the NH_2-MIL-101(Fe)@MIP, while the NH_2-MIL-101(Fe)@NIP does not. Thus, the above results strongly testify that the imprinting materials have been successfully prepared.

3.3. Optical properties

To explore the optical properties of synthesized materials, the fluorescence spectrophotometer was utilized to record the fluorescence signals. As clearly demonstrated by Fig. 3A, the spectra reveal that the optimal excitation and emission signals of NH_2-MIL-101(Fe) are positioned at 352 and 452 nm, respectively. In addition, the emission signal is heavily correlated with excitation wavelength utilized. As depicted in Fig. 3B, the excitation at 350 nm leads to strongest fluorescence signal, and the fluorescence signal gradually weakens as the excitation light deviates from optimum value. Visibly, the corresponding solution presents intensive blue light under 365 nm UV light (the inset in Fig. 3B).

Similar to NH_2-MIL-101(Fe), the NH_2-MIL-101(Fe)@MIP also shows the optimal excitation and emission signals at 352 and 452 nm, respectively (Fig. 3C). Besides, its emission signal is also heavily dependent on the excitation wavelength used (Fig. 3D), and the

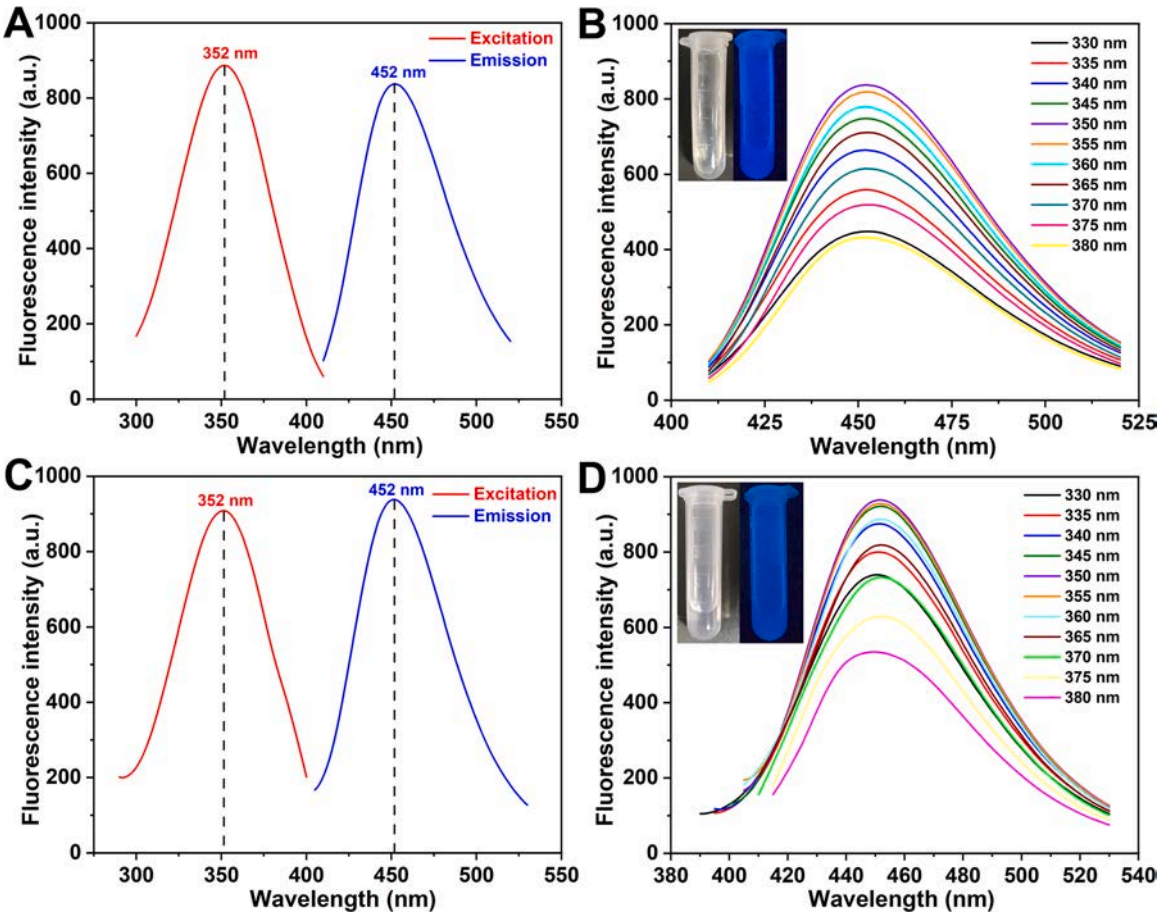

Fig. 3. (A) The excitation and emission spectra, and (B) the fluorescence spectra of NH_2-MIL-101(Fe) over the excitation wavelength range from 330 to 380 nm with an increment of 5 nm (the inset displays the corresponding physical photo under 365 nm UV lamp or not). (C) The fluorescence excitation and emission spectra, and (D) the fluorescence spectra of NH_2-MIL-101(Fe)@MIP over the excitation wavelength range from 330 to 380 nm with an increment of 5 nm (the inset displays the corresponding physical photo under 365 nm UV lamp or not).

corresponding solution also emits obvious blue light under 365 nm UV light (the inset in Fig. 3D). More interestingly, the NH_2-MIL-101(Fe)@NIP also exhibits virtually identical photoluminescence characteristics (Figs. S4 and S5). These results indicate that the coating of the imprinting layer has negligible effect on the intrinsic fluorescence properties of MOF.

3.4. Peroxidase-like properties

The peroxidase-like activity of prepared NH_2-MIL-101(Fe) was explored by utilizing OPD as a chromogenic substrate. As displayed in Fig. 4A, the NH_2-MIL-101(Fe) + H_2O_2 + OPD system has a well-defined peak approximately at 450 nm, which is ascribed to catalytic oxidation of OPD to form DAP. On the contrary, no distinct peak can be observed at 450 nm in several control systems. Correspondingly, it can be observed from the physical photo that the corresponding solution system changes from colorless to yellow, while the other three control systems have no color change. Instead of OPD, TMB can also work as another substrate to give the similar phenomenon (Fig. S6). To investigate the mechanism of the catalytic reaction, the electron paramagnetic resonance (EPR) was adopted to analyze the generated free radicals in the procedure of catalytic reaction. As shown in Fig. 4B, this classic characteristic peak of 1:2:2:1 should be ascribed to the generated hydroxyl radical (·OH) [40]. Compared with NH_2-MIL-101(Fe), the signal peak intensities of NH_2-MIL-101(Fe)@MIP and NH_2-MIL-101(Fe)@NIP reveal different degrees of decrease, which proves that the peroxidase-like activities of NH_2-MIL-101(Fe)@MIP and NH_2-MIL-101(Fe)@NIP decrease accordingly due to the coating of the imprinting layer. The catalytic reaction process is vividly described by Fig. 4C, NH_2-MIL-101(Fe) catalyzes the decomposition of H_2O_2 to produce hydroxyl radicals, which can oxidize the OPD to form fluorescent DAP.

To further study the peroxidase-like properties of NH_2-MIL-101(Fe), the steady-state kinetics tests were measured. As illustrated in Fig. S7, the Michaelis–Menten constant (K_m) towards TMB and H_2O_2 are determined to be 0.166 mM and 1.111 mM, respectively. Compared with HRP and other typical peroxidase mimics [41–44], the lower K_m values of prepared MOF material exhibits its better affinity to TMB and H_2O_2 substrates (Table S3).

Subsequently, the peroxidase-like activities of imprinting materials were also explored. As demonstrated by Fig. 4D, the peroxidase-like activities of NH_2-MIL-101(Fe)@MIP and NH_2-MIL-101(Fe)@NIP exhibit different degrees of reduction due to the coating of the imprinting layer. The former with abundant molecularly imprinted cavities can provide the channels for H_2O_2 to contact with NH_2-MIL-101(Fe) inside imprinting layer. Subsequently, internal NH_2-MIL-101(Fe) catalyzes decomposition of H_2O_2 to produce hydroxyl radicals to induce the oxidation of OPD to fluorescent DAP. Consequently, NH_2-MIL-101(Fe)@MIP still exhibits good peroxidase-like activity. In contrast, the latter without imprinted cavities hinders H_2O_2 passing through the imprinting layer to contact with NH_2-MIL-101(Fe), resulting in extremely weak enzyme activity. Meanwhile, the similar results are presented by utilizing TMB as a substrate instead of OPD (Fig. S8).

Besides, several experimental parameters including pH value, excitation wavelength, and reaction time were optimized. As depicted in

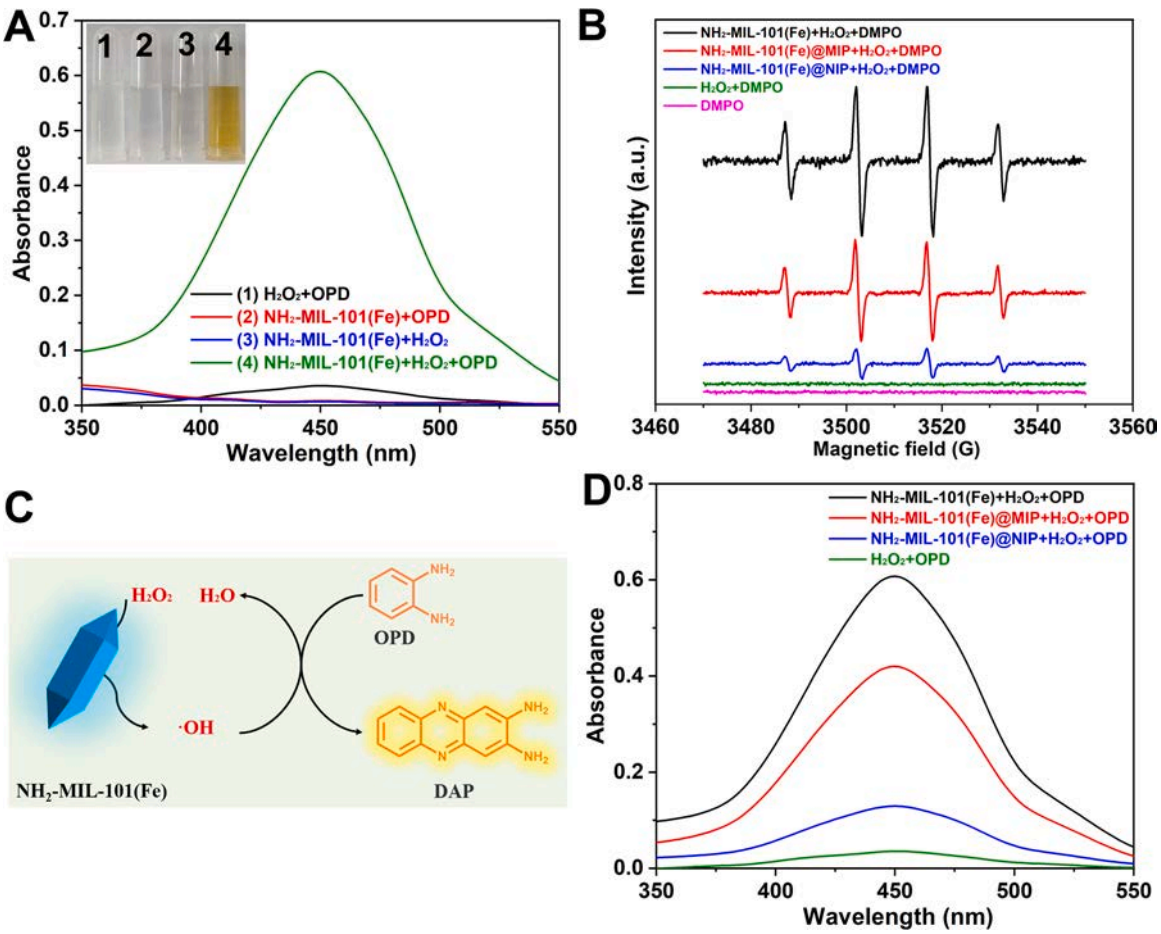

Fig. 4. (A) The UV–vis spectra of various systems (inset is the corresponding physical photo). (B) The EPR spectra of diverse systems. (C) The catalytic reaction mechanism. (D) The UV–vis spectra of different systems.

Fig. S9, the NH_2-MIL-101(Fe)@MIP supplies the highest peroxidase-like activity at pH 4.0. As the excitation signals change, the two peaks at 556 and 452 nm vary accordingly. Finally, 390 nm is determined as an optimal excitation signal considering the sensitivity and linear range of the ratiometric fluorescence sensor (Fig. S10). As confirmed by Fig. S11, the fluorescence signal of DAP increases with the prolongation of reaction time, while the intrinsic signal decreases. To coordinate the detection time and analysis performance, the reaction time is set to 20 min. Besides, the excellent robustness in harsh environment is also a highlight of nanozymes. To explore the robustness of prepared material under harsh environment, NH_2-MIL-101(Fe)@MIP was placed in environments with different pH and temperature conditions for 30 min. Subsequently, the peroxidase-like activity of NH_2-MIL-101(Fe)@MIP was measured under optimal experimental parameters. As demonstrated by Fig. S12 and Fig. S13, the NH_2-MIL-101(Fe)@MIP is still able to maintain high enzyme activity, indicating its good robustness under harsh environment. These outstanding features endow it a broader prospect in practical application.

3.5. Feasibility of the designed sensor for DA sensing

Fascinatingly, the NH_2-MIL-101(Fe)@MIP induces the oxidation of OPD to generate fluorescent DAP, which can cause the fluorescence changes of whole system. As confirmed by Fig. 5A, it presents an intrinsic peak at 452 nm when the excitation signal is 390 nm, which is attributed to the 2-NH_2-1,4-BDC ligand. After OPD and H_2O_2 are introduced, OPD can be catalytically oxidized to fluorescent DAP. Interestingly, a distinct signal emerges at about 556 nm, which should be attributed to the fluorescent DAP. Meanwhile, the intrinsic fluorescence signal (452 nm) is inhibited to a certain extent concurrently. To explore the mechanism of this phenomenon, the fluorescence signal of NH_2-MIL-101(Fe)@MIP and UV–vis absorption signal of DAP were measured. As displayed in Fig. 5B, the fluorescence signal (452 nm) evidently overlaps with the UV–vis absorption signal (450 nm). Thus, the suppression phenomenon of intrinsic fluorescence signal of NH_2-MIL-101(Fe)@MIP should be assigned to fluorescence inner filter effect (IFE) [45,46].

As displayed in Fig. 5C, NH_2-MIL-101(Fe)@MIP induces decomposition of H_2O_2 to produce hydroxyl radicals, which can oxidize OPD to form fluorescent DAP. When the excitation signal is set to 390 nm, two notable emission peaks are generated at 452 nm and 556 nm, which are ascribed to intrinsic signal of material and fluorescence signal presented by DAP, respectively (Fig. 5D). After the addition of DA, the molecularly imprinted cavities on the NH_2-MIL-101(Fe)@MIP can specifically adsorb DA because of the high selectivity offered by MIT, which blocks the passage of H_2O_2 through the imprinted layer, and subsequently inhibits the production of hydroxyl radicals. Consequently, the amount of fluorescent DAP generated by the oxidation of OPD through hydroxyl radicals is reduced [47]. In the end, the fluorescence signal of DAP decreases significantly, and the one (452 nm) of NH_2-MIL-101(Fe)@MIP is recovered due to the weakening of the IFE between the two (Fig. 5D).

In contrast, the NH_2-MIL-101(Fe)@NIP without imprinted cavities hinders the contact between the outside H_2O_2 and inside NH_2-MIL-101(Fe), resulting in extremely weak enzyme activity (Fig. 5E). As a result, only an exceeding small amount of fluorescent DAP is generated and emerges an extremely weak peak at 556 nm. Nevertheless, the intrinsic fluorescence signal (452 nm) is significantly enhanced owing to greatly weakening of the IFE between the two. After the introduction of DA, a

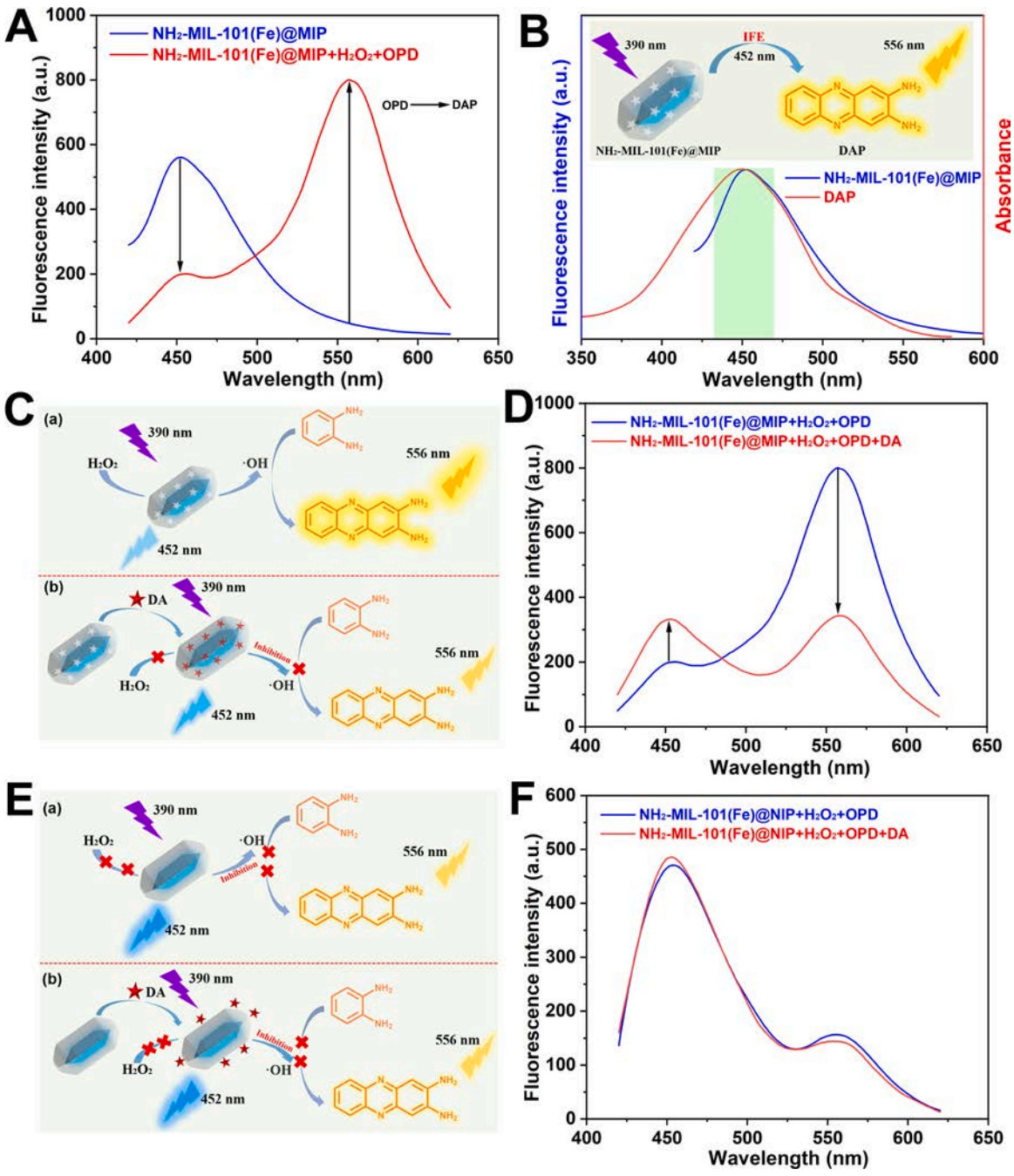

Fig. 5. (A) The fluorescence spectra of NH_2-MIL-101(Fe)@MIP and NH_2-MIL-101(Fe)@MIP + H_2O_2 + OPD systems. (B) The fluorescence inner filter effect between NH_2-MIL-101(Fe)@MIP and DAP. (C) The effect of DA on the signals of the NH_2-MIL-101(Fe)@MIP + H_2O_2 + OPD system, and (D) the corresponding fluorescence spectra. (E) The effect of DA on the signals of the NH_2-MIL-101(Fe)@NIP + H_2O_2 + OPD system, and (F) the corresponding fluorescence spectra.

few DA may nonspecifically adhere to the surface of NH_2-MIL-101(Fe)@NIP, which gives negligible effect on the fluorescence of the whole system (Fig. 5F). These outcomes testify that the designed sensor can be well applied to fluorescence sensing of DA.

3.6. High performance ratiometric fluorescent sensing of DA

Before analysis, possible influential factors in the whole system were considered. As displayed in Fig. S14, the fluorescence ratio of F_{556}/F_{452} decreases rapidly in the first 5 min and reaches dynamic equilibrium in about 10 min. Thus, the 10 min is determined as the optimal incubation time in the following experiments. Additionally, the DA or OPD reveals no impact on the intrinsic fluorescence (452 nm) (Fig. S15 and Fig. S16), which also strong certify that the change of intrinsic fluorescence (452 nm) is caused by IFE between the generated fluorescent DAP and NH_2-MIL-101(Fe)@MIP, and further confirm feasibility of designed sensor.

After optimizing several experimental parameters and excluding some possible interference factors, we employed the fabricated the ratiometric fluorescent sensor for quantitative sensing of DA under optimal experimental conditions. As depicted in Fig. 6A, the intrinsic signal (452 nm) gradually increases with the increase of DA concentration, while the peak signal (556 nm) of fluorescent DAP decreases instead. Subsequently, the fluorescence signal values at 452 nm and 556 nm are recorded, and the fluorescence ratio of F_{556}/F_{452} is taken as the readout, displaying the relationship between F_{556}/F_{452} and the level

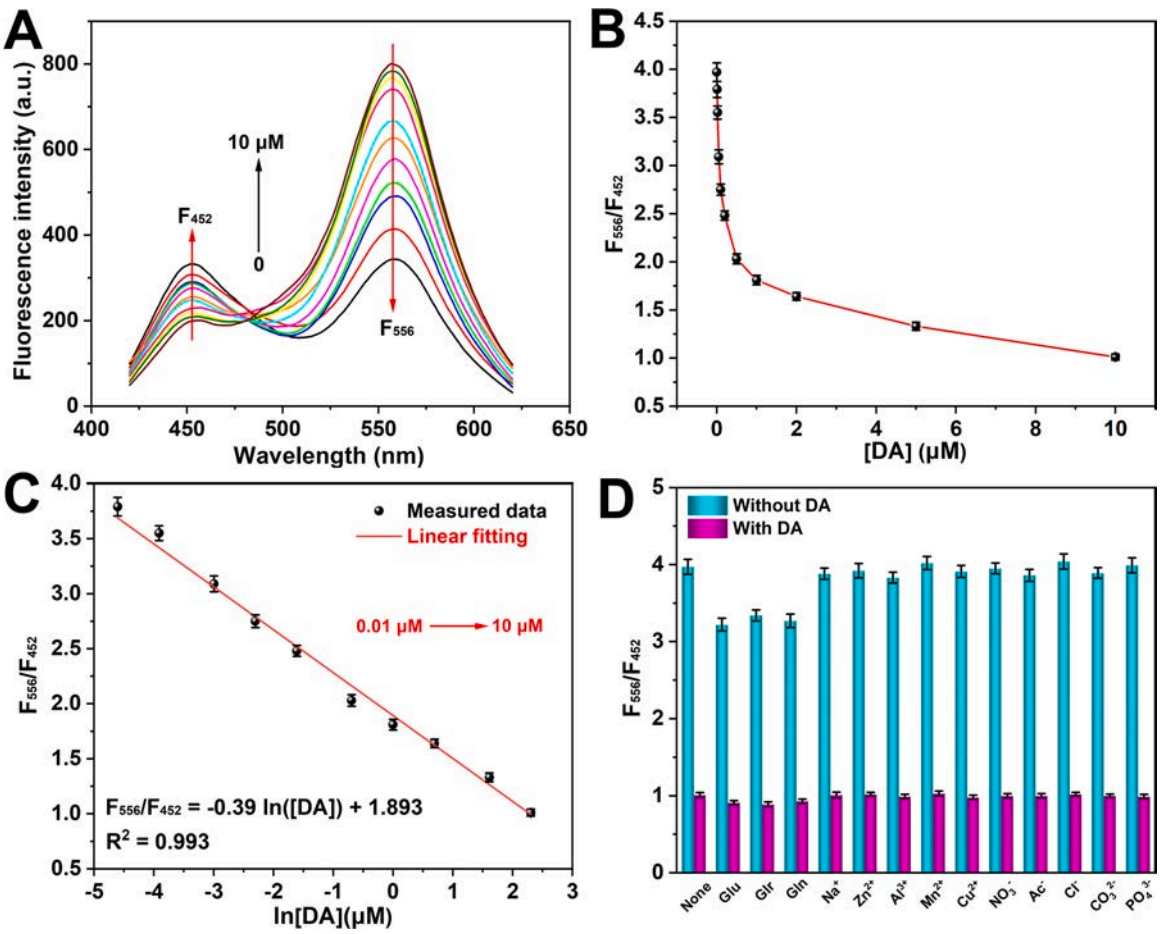

Fig. 6. (A) The fluorescence spectra of NH_2-MIL-101(Fe)@MIP + H_2O_2 + OPD system with diverse levels of DA. (B) The correlation of F_{556}/F_{452} to the level of DA. (C) The fitting curve between F_{556}/F_{452} and the content of DA. (D) The selectivity and interference experiments of the ratiometric fluorescent sensor sensing for DA sensing (10 μM) with diverse interfering substances (10 mg L^{-1}).

of DA (Fig. 6B). Amazingly, the fluorescence ratio of F_{556}/F_{452} is well linear with logarithm of DA level ranging from 0.01 to 10 μM, supplying a fitting equation: $F_{556}/F_{452} = -0.39 \ln[DA] + 1.893$ ($R^2 = 0.993$), and the limit of detection (LOD) towards DA is calculated as low as 8.2 nM based on the signal-to-noise of three (S/N = 3) (Fig. 6C). Such a low LOD exhibits great application prospects in rapid detection methods.

The selectivity and specificity are the crucial parameters for evaluating the analytical performance of the fabricated ratiometric fluorescent sensor in complex samples. To verify the selectivity and specificity of the fabricated ratiometric fluorescent sensor towards DA, some possible co-existing interferents including Glu, Glr, Gln, Na^+, Zn^{2+}, Al^{3+}, Mn^{2+}, Cu^{2+}, NO^{3-}, Ac^-, Cl^-, CO_3^{2-}, and PO_4^{3-} were employed. As illustrated in Fig. 6D, the possible co-existing interferents except for Glu, Glr, and Gln demonstrate negligible impacts towards the F_{556}/F_{452}. Owing to the similar chemical structure with DA, the Glu, Glr, and Gln can also affect the F_{556}/F_{452} in whole system. However, compared with DA, the Glu, Glr, and Gln present extremely weak influences on F_{556}/F_{452}. Moreover, when DA coexists with each interferent, the fluorescence ratio of F_{556}/F_{452} shows negligible changes compared with DA alone. These results illustrate that the fabricated ratiometric fluorescent sensor can provide outstanding selectivity and specificity for DA sensing thanks to MIT.

To further demonstrate the advantages of the fabricated ratiometric fluorescent sensor, some previously reported classical methods were compared with our sensing strategy and listed in Table S4 [15,16, 48–50]. Quite evidently, our proposed ratiometric fluorescent strategy is comparable to some reported methods in terms of linear range and LOD. However, the developed ratiometric fluorescent sensor with excellent sensitivity only utilizes cheap composite signal probe, which is attributed to inexpensive and easily available bifunctional NH_2-MIL-101(Fe). Besides, MIT instead of expensive antibodies can endow our developed ratiometric fluorescent sensor outstanding selectivity and specificity. More attractively, our proposed ratiometric fluorescent sensor with good stability can maintain almost constant analytical performance within 30 days (Fig. S17). These unique superiorities endue our sensor enormous potential in practical applications.

The fabricated ratiometric fluorescent sensor was further applied to quantitatively analyze DA in lake water and shellfish samples by spike and recovery test to verify the reliability of one. After pretreatment, the DA spiked in the lake water and shellfish samples were analyzed by our ratiometric fluorescent sensor. As demonstrated by Table S5, the proposed sensing strategy based on ratiometric fluorescence can supply outstanding recoveries (92%–108%) for quantitative sensing of DA in spiked real samples, verifying the good reliability of our sensors in sensing the analyte in actual samples.

4. Conclusions

In short, we have integrated the bifunctional NH_2-MIL-101(Fe) with molecular imprinting to design a ratiometric fluorescent sensor for DA sensing with the LOD down to the nM level. Such a high sensitivity should be attributed to composite fluorescent probe (NH_2-MIL-101(Fe)). Simultaneously, the introduction of MIT instead of expensive antibodies can endow our ratiometric fluorescent sensor outstanding selectivity and specificity for DA detection. The excellent outcomes of the spiked tests for DA in shellfish and lake water samples testify its considerable

practical application promise in marine toxins monitoring and rapid environmental analysis. More importantly, this research inspires the combined application of multifunctional MOF nanozymes and molecular imprinting for integrated sensing.

CRediT authorship contribution statement

Linjie Wang: Conceptualization, Methodology, Data curation, Writing – original draft. **Lejuan Wen:** Formal analysis, Investigation, Methodology, Validation, Writing – review & editing. **Shujun Zheng:** Formal analysis, Validation. **Feifei Tao:** Resources. **Jie Chao:** Resources. **Fei Wang:** Visualization, Supervision. **Caolong Li:** Supervision, Project administration, Funding acquisition.

Declaration of Competing Interest

The authors declare that they have no known competing financial interests or personal relationships that could have appeared to influence the work reported in this paper.

Acknowledgements

The authors thank the financial support from the National Key Research and Development Program (2019YFC0312602) as well as the Jiangsu Overseas Visiting Scholar Program for University Prominent Young & Middle-aged Teachers and Presidents. The authors also appreciate the Natural Science Foundation of China (51372154).

Appendix A. Supporting information

Supplementary data associated with this article can be found in the online version at doi:10.1016/j.snb.2022.131688.

References

[1] Y. Li, C.X. Huang, G.S. Xu, N. Lundholm, S.T. Teng, H. Wu, Z. Tan, Pseudo-nitzschia simulans sp. nov.(Bacillariophyceae), the first domoic acid producer from Chinese waters, Harmful Algae 67 (2017) 119–130.
[2] C. Tenorio, G. Álvarez, S. Quijano-Scheggia, M. Perez-Alania, N. Arakaki, M. Araya, F. Álvarez, J. Blanco, E. Uribe, First report of domoic acid production from Pseudo-nitzschia multistriata in Paracas Bay (Peru), Toxins 13 (2021) 408.
[3] L. Mos, Domoic acid: a fascinating marine toxin, Environ. Toxicol. Pharmacol. 9 (2001) 79–85.
[4] F.M. Van Dolah, Marine algal toxins: origins, health effects, and their increased occurrence, Environ. Health Perspect. 108 (2000) 133–141.
[5] F. Farabegoli, L. Blanco, L.P. Rodríguez, J.M. Vieites, A.G. Cabado, Phycotoxins in marine shellfish: origin, occurrence and effects on humans, Mar. Drugs 16 (2018) 188.
[6] Y. Ji, G. Yan, G. Wang, J. Liu, Z. Tang, Y. Yan, J. Qiu, L. Zhang, W. Pan, Y. Fu, Prevalence and distribution of domoic acid and cyclic imines in bivalve mollusks from Beibu Gulf, China J. Hazard. Mater. 423 (2022), 127078.
[7] J.M. Maucher, J.S. Ramsdell, Ultrasensitive detection of domoic acid in mouse blood by competitive ELISA using blood collection cards, Toxicon 45 (2005) 607–613.
[8] W.-H. Zhou, X.-C. Guo, H.-Q. Zhao, S.-X. Wu, H.-H. Yang, X.-R. Wang, Molecularly imprinted polymer for selective extraction of domoic acid from seafood coupled with high-performance liquid chromatographic determination, Talanta 84 (2011) 777–782.
[9] J. Regueiro, G. Álvarez, A. Mauriz, J. Blanco, High throughput analysis of amnesic shellfish poisoning toxins in bivalve molluscs by dispersive solid-phase extraction and high-performance liquid chromatography using a monolithic column, Food Chem. 127 (2011) 1884–1891.
[10] X.-W. Zhang, Z.-X. Zhang, Quantification of domoic acid in shellfish samples by capillary electrophoresis-based enzyme immunoassay with electrochemical detection, Toxicon 59 (2012) 626–632.
[11] F. Kvasnička, R. Ševčík, M. Voldřich, Determination of domoic acid by on-line coupled capillary isotachophoresis with capillary zone electrophoresis, J. Chromatogr. A 1113 (2006) 255–258.
[12] R.W. Litaker, T.N. Stewart, B.-T.L. Eberhart, J.C. Wekell, V.L. Trainer, R.M. Kudela, P.E. Miller, A. Roberts, C. Hertz, T.A. Johnson, Rapid enzyme-linked immunosorbent assay for detection of the algal toxin domoic acid, J. Shellfish Res. 27 (2008) 1301–1310.
[13] F.-Y. Yu, B.-H. Liu, T.-S. Wu, T.-F. Chi, M.-C. Su, Development of a sensitive enzyme-linked immunosorbent assay for the determination of domoic acid in shellfish, J. Agric. Food Chem. 52 (2004) 5334–5339.
[14] M. Jiang, J. Tang, N. Zhou, J. Liu, F. Tao, F. Wang, C. Li, Rapid electrochemical detection of domoic acid based on polydopamine/reduced graphene oxide coupled with in-situ imprinted polyacrylamide, Talanta 236 (2022), 122885.
[15] J.L. Nelis, D. Migliorelli, L. Mühlebach, S. Generelli, L. Stewart, C.T. Elliott, K. Campbell, Highly sensitive electrochemical detection of the marine toxins okadaic acid and domoic acid with carbon black modified screen printed electrodes, Talanta 228 (2021), 122215.
[16] L. Dan, H.-F. Wang, Mn-doped ZnS quantum dot imbedded two-fragment imprinting silica for enhanced room temperature phosphorescence probing of domoic acid, Anal. Chem. 85 (2013) 4844–4848.
[17] J. Ping, Z. Fan, M. Sindoro, Y. Ying, H. Zhang, Recent advances in sensing applications of two-dimensional transition metal dichalcogenide nanosheets and their composites, Adv. Funct. Mater. 27 (2017), 1605817.
[18] D. Zhao, J. Li, C. Peng, S. Zhu, J. Sun, X. Yang, Fluorescence immunoassay based on the alkaline phosphatase triggered in situ fluorogenic reaction of O-phenylenediamine and ascorbic acid, Anal. Chem. 91 (2019) 2978–2984.
[19] Z. Lian, M. Zhao, J. Wang, R.-C. Yu, Dual-emission ratiometric fluorescent sensor based molecularly imprinted nanoparticles for visual detection of okadaic acid in seawater and sediment, Sens. Actuators, B 346 (2021), 130465.
[20] Y. Xu, J. Xue, Q. Zhou, Y. Zheng, X. Chen, S. Liu, Y. Shen, Y. Zhang, The Fe-N-C nanozyme with both accelerated and inhibited biocatalytic activities capable of accessing drug–drug interactions, Angew. Chem. 132 (2020) 14606–14611.
[21] P. Liu, M. Zhao, H. Zhu, M. Zhang, X. Li, M. Wang, B. Liu, J. Pan, X. Niu, Dual-mode fluorescence and colorimetric detection of pesticides realized by integrating stimulus-responsive luminescence with oxidase-mimetic activity into cerium-based coordination polymer nanoparticles, J. Hazard. Mater. 423 (2022), 127077.
[22] X. Niu, X. Li, Z. Lyu, J. Pan, S. Ding, X. Ruan, W. Zhu, D. Du, Y. Lin, Metal–organic framework based nanozymes: promising materials for biochemical analysis, Chem. Commun. 56 (2020) 11338–11353.
[23] L. Liu, H. Jiang, X. Wang, Functionalized gold nanomaterials as biomimetic nanozymes and biosensing actuators, TrAC, Trends Anal. Chem. 143 (2021), 116376.
[24] L. Hou, Y. Qin, J. Li, S. Qin, Y. Huang, T. Lin, L. Guo, F. Ye, S. Zhao, A ratiometric multicolor fluorescence biosensor for visual detection of alkaline phosphatase activity via a smartphone, Biosens. Bioelectron. 143 (2019), 111605.
[25] F. Wang, L. Chen, D. Liu, W. Ma, P. Dramou, H. He, Nanozymes based on metal-organic frameworks: construction and prospects, TrAC, Trends Anal. Chem. 133 (2020), 116080.
[26] S. Li, X. Liu, H. Chai, Y. Huang, Recent advances in the construction and analytical applications of metal-organic frameworks-based nanozymes, TrAC, Trends Anal. Chem. 105 (2018) 391–403.
[27] Z. Yang, W. Zhang, Y. Yin, W. Fang, H. Xue, Metal-organic framework-based sensors for the detection of toxins and foodborne pathogens, Food Control (2021), 108684.
[28] D. Jiang, D. Ni, Z.T. Rosenkrans, P. Huang, X. Yan, W. Cai, Nanozyme: new horizons for responsive biomedical applications, Chem. Soc. Rev. 48 (2019) 3683–3704.
[29] P. Liu, X. Li, X. Xu, K. Ye, L. Wang, H. Zhu, M. Wang, X. Niu, Integrating peroxidase-mimicking activity with photoluminescence into one framework structure for high-performance ratiometric fluorescent pesticide sensing, Sens. Actuators, B 328 (2021), 129024.
[30] J. Huang, Y. Wu, J. Cong, J. Luo, X. Liu, Selective and sensitive glycoprotein detection via a biomimetic electrochemical sensor based on surface molecular imprinting and boronate-modified reduced graphene oxide, Sens. Actuators, B 259 (2018) 1–9.
[31] L. Fang, M. Jia, H. Zhao, L. Kang, L. Shi, L. Zhou, W. Kong, Molecularly imprinted polymer-based optical sensors for pesticides in foods: recent advances and future trends, Trends Food Sci. Technol. 116 (2021) 387–404.
[32] X. Xu, Z. Luo, K. Ye, X. Zou, X. Niu, J. Pan, One-pot construction of acid phosphatase and hemin loaded multifunctional metal–organic framework nanosheets for ratiometric fluorescent arsenate sensing, J. Hazard. Mater. 412 (2021), 124407.
[33] K. Nemoto, T. Kubo, M. Nomachi, T. Sano, T. Matsumoto, K. Hosoya, T. Hattori, K. Kaya, Simple and effective 3D recognition of domoic acid using a molecularly imprinted polymer, J. Am. Chem. Soc. 129 (2007) 13626–13632.
[34] W. Xu, Y. Kang, L. Jiao, Y. Wu, H. Yan, J. Li, W. Gu, W. Song, C. Zhu, Tuning atomically dispersed Fe sites in metal–organic frameworks boosts peroxidase-like activity for sensitive biosensing, Nano-Micro Lett. 12 (2020) 1–12.
[35] X. Li, W. Guo, Z. Liu, R. Wang, H. Liu, Quinone-modified NH_2-MIL-101(Fe) composite as a redox mediator for improved degradation of bisphenol A, J. Hazard. Mater. 324 (2017) 665–672.
[36] P. Huang, L. Yao, Q. Chang, Y. Sha, G. Jiang, S. Zhang, Z. Li, Room-temperature preparation of highly efficient NH_2-MIL-101(Fe) catalyst: the important role of $–NH_2$ in accelerating Fe(III)/Fe(II) cycling, Chemosphere 291 (2021), 133026.
[37] L. Tian, H. Guo, J. Li, L. Yan, E. Zhu, X. Liu, K. Li, Fabrication of a near-infrared excitation surface molecular imprinting ratiometric fluorescent probe for sensitive and rapid detecting perfluorooctane sulfonate in complex matrix, J. Hazard. Mater. 413 (2021), 125353.
[38] Z. Li, H. Xu, D. Wu, J. Zhang, X. Liu, S. Gao, Y. Kong, Electrochemical chiral recognition of tryptophan isomers based on nonionic surfactant-assisted molecular imprinting sol–gel silica, ACS Appl. Mater. Interfaces 11 (2018) 2840–2848.
[39] L. Wang, X. Xu, X. Niu, J. Pan, Colorimetric detection and membrane removal of arsenate by a multifunctional L-arginine modified FeOOH, Sep. Purif. Technol. 258 (2021), 118021.

[40] Y. Zhang, Y.-S. Feng, X.-H. Ren, X.-W. He, W.-Y. Li, Y.-K. Zhang, Bimetallic molecularly imprinted nanozyme: dual-mode detection platform, Biosens. Bioelectron. 196 (2022), 113718.
[41] L. Gao, J. Zhuang, L. Nie, J. Zhang, Y. Zhang, N. Gu, T. Wang, J. Feng, D. Yang, S. Perrett, Intrinsic peroxidase-like activity of ferromagnetic nanoparticles, Nat. Nanotechnol. 2 (2007) 577–583.
[42] L. Hu, Y. Yuan, L. Zhang, J. Zhao, S. Majeed, G. Xu, Copper nanoclusters as peroxidase mimetics and their applications to H_2O_2 and glucose detection, Anal. Chim. Acta 762 (2013) 83–86.
[43] S. Singh, K. Mitra, R. Singh, A. Kumari, S.K.S. Gupta, N. Misra, P. Maiti, B. Ray, Colorimetric detection of hydrogen peroxide and glucose using brominated graphene, Anal. Methods 9 (2017) 6675–6681.
[44] D. Zhou, K. Zeng, M. Yang, Gold nanoparticle-loaded hollow Prussian blue nanoparticles with peroxidase-like activity for colorimetric determination of L-lactic acid, Microchim. Acta 186 (2019) 1–7.
[45] S. Li, X. Hu, Q. Chen, X. Zhang, H. Chai, Y. Huang, Introducing bifunctional metal-organic frameworks to the construction of a novel ratiometric fluorescence sensor for screening acid phosphatase activity, Biosens. Bioelectron. 137 (2019) 133–139.
[46] X. Yan, H. Li, X. Han, X. Su, A ratiometric fluorescent quantum dots based biosensor for organophosphorus pesticides detection by inner-filter effect, Biosens. Bioelectron. 74 (2015) 277–283.
[47] Z. Zhang, Y. Liu, P. Huang, F.-Y. Wu, L. Ma, Polydopamine molecularly imprinted polymer coated on a biomimetic iron-based metal–organic framework for highly selective fluorescence detection of metronidazole, Talanta 232 (2021), 122411.
[48] C. Müller, B. Glamuzina, I. Pozniak, K. Weber, D. Cialla, J. Popp, S.C. Pînzaru, Amnesic shellfish poisoning biotoxin detection in seawater using pure or amino-functionalized Ag nanoparticles and SERS, Talanta 130 (2014) 108–115.
[49] L. Micheli, A. Radoi, R. Guarrina, R. Massaud, C. Bala, D. Moscone, G. Palleschi, Disposable immunosensor for the determination of domoic acid in shellfish, Biosens. Bioelectron. 20 (2004) 190–196.
[50] W.-H. Zhou, S.-F. Tang, Q.-H. Yao, F.-R. Chen, H.-H. Yang, X.-R. Wang, A quartz crystal microbalance sensor based on mussel-inspired molecularly imprinted polymer, Biosens. Bioelectron. 26 (2010) 585–589.

Linjie Wang is a doctoral candidate at China Pharmaceutical University, and he focuses on the fabrication of sensing systems using nanozymes.

Lejuan Wen is a master candidate under the supervision of Dr. Li and Dr. Wang, and she is interested in detection of marine toxins based on nanozymes.

Shujun Zheng is a master candidate under the supervision of Dr. Li and Dr. Wang, and she focuses on biochemical analysis based on nanozymes.

Feifei Tao is an associated professor at Shaoxing University. Her research interests include fundamental electrochemistry, electrocatalysis and electrochemical analysis.

Jie chao is a professor at Southeast University, and he focuses on the disease diagnosis and treatment.

Fei Wang is an associated professor at China Pharmaceutical University. He shows his favor in the fabrication of functional nanomaterials, and is deeply absorbed in the corresponding applications of medical analysis and fluorescence devices.

Caolong Li is a professor at China Pharmaceutical University, and he focuses on the functionalization of nanomaterials in medical analysis, biomedical imaging, gas sensing, and fluorescence devices.